Three-dimensional Free Electron Laser numerical simulations for a laser wiggler in the quatum regime

A. Schiavi[1], R. Bonifacio[2,4], N. Piovella[2,3], M.M. Cola[2,3], and L. Volpe[2,3]

[1] *Dipartimento di Energetica, Università di Roma "La Sapienza" and INFN, Via Scarpa 14, I-00161 Roma, Italy*
[2] *Dipartimento di Fisica, Università Degli Studi di Milano, via Celoria 16, I-20133 Milano, Italy*
[3] *INFN - sezione di Milano - via Celoria 16, I-20133 Milano, Italy*
[4] *Centro Brasileiro de Pesquisas Físicas, Rio de Janeiro - Brasil*

Abstract

A compact tunable source of soft X-rays could be realized combining a state-of-the-art electron source with an intense couterpropagating laser pulse. If the source is operated in the quatum regime, the theoretical model predicts high monochromaticity (single-spike) and unprecedented temporal coherence for the emitted radiation. Here we present numerical simulations of the complete quantum model for an FEL with a laser wiggler in three spatial dimensions, based on a discrete Wigner function formalism taking into account the longitudinal momentum quantization. The numerical model includes the complete spatial and temporal evolution of the electron and radiation beams, with an explicit description of diffraction, propagation, laser wiggler profile and emittance effects. The contribution of each interaction term is studied independently, and the 3D results are contrasted with the 1D quantum FEL model neglecting transverse effects. Finally the parameter space for possible experiments is characterized, and a particular experimental case is discussed in detail.

1. Introduction

In the quest of tunable and bright X-ray sources a novel approach has been recently proposed consisting in operating a Free-Electron laser (FEL) in a weak interaction regime where the discreteness of momentum exchange between electrons and radiation becomes relevant. In this regime, called quantum regime (1; 2), the theoretical model predicts the possibility to operate in the self amplified spontaneous emission (SASE) mode obtaining a nearly single spike spectrum and extremely long coherent X-ray pulses, overcoming thus many limitations of conventional FEL sources (3; 4; 5). A discussion of the main features of the longitudinal dynamics of a quantum FEL (QFEL) in the SASE mode operation is presented elsewhere in these Proceedings (6), as well as a description of the inclusion in the model of the transverse dynamics based on the Wigner function for the electron beam (7). It has been shown that, in order to realize a QFEL, a laser wiggler must be used (8; 9). Such a choice sets some stringent conditions on the electron and laser beam parameters (10), which should be verified by numerical 3D simulations. A numerical code `QFEL3D` has been

developed for integrating the the coupled QFEL equations describing the interaction of the electrons with the radiation field. The numerical scheme is based on a Fourier decomposition of the Wigner function and on finite-difference (FD) integration of the motion equations on a Cartesian three-dimensional spatial grid. A combination of different integration schemes were adopted in an operator splitting algorithm. An explicit FD scheme coupled to a Runge-Kutta stepper was used for integrating the interaction of the field and the electron bunch (11). A cubic-interpolation propagation (CIP) method was implemented for solving the advection equation of the radiation field in the electron bunch rest frame (12). The beam transverse motion was tracked using a 2D Vlasov solver. A linear domain decomposition technique was used for distributing the computation over a cluster of processors. Since the computation involved large complex valued arrays of rank up to $N = 7$, the computational kernel was written in `F90`. The communication between different nodes was implemented using the MPI library. The front-end, the disk IO and link with the graphics libraries was implemented using a `C++` driver. In this work we present the simulations results of QFEL

model for a particular set of parameter, which indicate the path to a laser wiggler experiment in the near future (10). In the first section the 1D model is introduced and the consistency of the new Wigner formulation with the previous Schrödinger equation approach is assessed. The parameter space is then characterized and the choice of the working point is explained. A study of the 1D energy output is then presented for determining the relation between the steady-state solution and the average properties of the SASE operation mode. In the subsequent section the results of 3D simulations are presented, focussing on the relative importance of the new dynamical terms. The conditions necessary to preserve the FEL resonance are then outlined, and finally the conclusions are drawn.

2. 1D model

It has been shown that a Quantum FEL can be described using a Wigner function approach in the 1D limit by the following equations (13):

$$\frac{\partial w_s}{\partial \bar{z}} = -\frac{s}{\bar{\rho}^{3/2}}\frac{\partial w_s}{\partial \theta} + \left(Ae^{i\theta} + A^*e^{-i\theta}\right)\left(w_{s+\frac{1}{2}} - w_{s-\frac{1}{2}}\right)(1)$$

$$\frac{\partial A}{\partial \bar{z}} + \frac{\partial A}{\partial z_1} = \sum_{m=-\infty}^{+\infty}\int_{-\pi}^{+\pi} d\theta e^{-i\theta} w_{m+\frac{1}{2}} + i\delta A \qquad (2)$$

Here the w_s are the components of the discrete Wigner function (14) labelled by the half-integer index $s \in \mathbb{Z}/2$. The variables and the parameters are defined accordingly to the description of the model presented in (13). In particular $\theta = (k_r + k_L)z - c(k_r - k_L)t - \delta\bar{z}$ is the electron phase, where $k_L = 2\pi/\lambda_L$ and $k_r = 2\pi/\lambda_r$ are the laser and radiation wave numbers, respectively; $p = mc(\gamma - \gamma_0)/(\hbar k_r)$ is the longitudinal momentum, in units of the photon recoil momentum, $\hbar k_r$, and $\delta = mc(\gamma_0 - \gamma_r)/(\bar{\rho}\hbar k_r)$ is the detuning, where γ_0 and $\gamma_r = [\lambda_L(1 + a_0^2)/4\lambda_r]^{1/2}$ are the initial and resonant electron energy in mc^2 units, respectively; the position along the wiggler $\bar{z} = z/L_g$ is expressed in gain length units $L_g = \lambda_L/(8\pi\rho\sqrt{\rho})$, and the electron position along the beam is $z_1 = (z - v_r t)/(\beta_r L_c)$, where $v_r = c\beta_r$ is the resonant velocity and $L_c = \lambda_r/(4\pi\rho\sqrt{\rho})$ is the cooperation length; $\rho = (1/2\gamma_r)(I/I_A)^{1/3}(\lambda_L a_0/4\pi\sigma)^{2/3}$ is the FEL parameter, I is the beam peak current, $I_A \approx 17kA$ is the Alfvèn current, σ is the transverse rms beam size; $a_0 = eE_0/mc^2k_L$ and E_0 is the laser electric field; A is the slowly varying amplitude of the radiation field, defined such that $|A|^2 = \epsilon_0|E_r|^2/(\hbar\omega_r n_b)$ is the average number of photons emitted per electron in the electron beam volume, E_r is the radiation electric field, $n_b = I/(2\pi\sigma^2ec)$ is the electron density and $\omega_r = ck_r$. The QFEL parameter $\bar{\rho} = \rho(mc\gamma_r/\hbar k_r)$ is approximately equal to the ratio between the maximum classical momentum spread (of the order of $mc\gamma_r\rho$) and the photon recoil momentum $\hbar k_r$, and yields also the maximum number of photons emitted per electron in a high-gain classical FEL.

It is worthwhile to recall that the above definitions are consistent with a electromagnetic wiggler realized, for instance, by a counter-propagating circularly polarized laser pulse. The basic equations were further rescaled and transformed before numerical implementation. Performing a constant phase shift on the dynamical variables w_s and A, the detuning term $\propto \delta$ is moved from the field equation onto the electron beam equation. Then the Wigner components, which are functions of the periodic electron phase θ, are expanded in a Fourier series $w_s(\theta, \bar{z}; z_1) = \frac{1}{2\pi}\sum_{k=-\infty}^{\infty} w_s^k(\bar{z}; z_1)e^{ik\theta}$. We finally obtain the equations that were solved numerically in the code

$$\frac{\partial w_s^k}{\partial \bar{z}} = -ik\left[\frac{s}{\bar{\rho}^{3/2}} + \delta\right]w_s^k$$
$$+A\left[w_{s+1/2}^{k-1} - w_{s-1/2}^{k-1}\right] + A^*\left[w_{s+1/2}^{k+1} - w_{s-1/2}^{k+1}\right] (3)$$

$$\frac{\partial A}{\partial \bar{z}} + \frac{\partial A}{\partial z_1} = \sum_{m=-\infty}^{+\infty} w_{m+\frac{1}{2}}^1 \qquad (4)$$

This new set of equations were integrated both in the classical ($\bar{\rho} >> 1$) and in the quantum regime ($\bar{\rho} < 1$) and the solution was contrasted with the predictions of a previous model based on a Schrödinger equation for the electron beam matter wave interaction with the radiation field(1). A striking perfect match was found within the numerical precision of the computer hardware, confirming that the two descriptions are indeed equivalent as far as the quantized longitudinal FEL dynamics is concerned. Figure 1 presents the evolution along the wiggler of the radiation field A and the bunching parameter b for a steady-state run with $\bar{\rho} = 0.1$. The electron beam had an initial bunching $b_0 = 0.01$ and no radiation seed was present. It is possible to see in the linear scale the typical periodic pulsing of the radiation field, and that A peaks at the value of 1, consistently with the quantum scaling. Solid lines in the plot refer to the Wigner model outlined above, whereas the markers correspond the Schrödinger equation model.
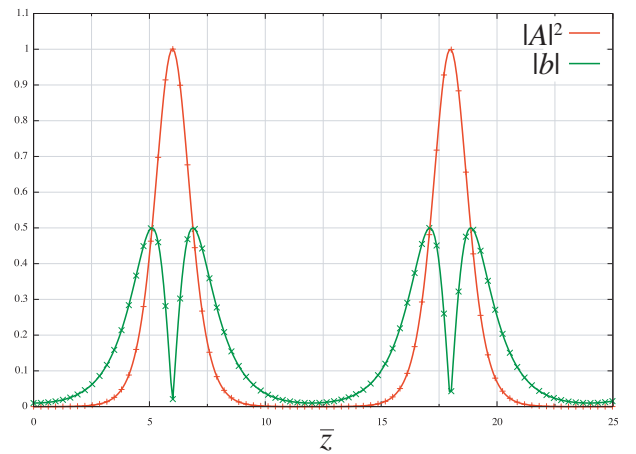

Fig. 1. Steady-state 1D models for $\bar{\rho} = 0.1$. Comparison of the Wigner function model (solid lines) with the Schrödinger equation model (markers).

2.1. Definition of the working point

For exploring the QFEL dynamics with a laser wiggler we chose a value of $\bar{\rho} = 0.2$, since this value lays in the quantum regime ($\bar{\rho} < 0.4$), and the gain length is not exceedingly long for experimental purposes. We chose a laser wavelength $\lambda_L = 1\mu m$ (representative for instance of a Nd:glass laser system), and we looked for an output resonant wavelength $\lambda_r = 2$ Å. The mean electron energy was set to 18 MeV ($\gamma_r = 36$). The electron beam had a beam waist $\sigma = 10\mu m$, while the minimum rms laser radius R was set to $20\mu m$. With these parameters, and under the assumption of transverse flat-top profiles for both the electron beam and the laser wiggler, it is possible to draw, using the relations obtained in (10), the contour plots for the quantum FEL parameter $\bar{\rho}$ and for the gain length L_g as a function of the laser power and of the beam current. Figure 2 shows that the desired $\bar{\rho} = 0.2$ can be obtained for a laser power in the range $1-10$ TW, which is easily accessible with present-day laser technology, while at the same time keeping the beam current below 1 kA, in order to avoid space charge instabilities as much as possible. The gain length is comprised between 1 and 2 mm in that parameter window, as shown in Figure 3. In order to keep the requirements on the laser system to a minimum, the chosen working point was defined by a laser power of 1 TW and a beam current of 884 A, corresponding to $\bar{\rho} = 0.2$ and $L_g = 1.3$mm. With this choice, the beam was 586 cooperation lengths long. The interaction was taken over 10 gain lengths ($\bar{z}_{max} = c\tau_{int}/L_g = 10$), with the beam waist in the middle, $\bar{z}_0 = 5$. The minimum duration of the laser pulse is therefore $\tau_L = 20\,L_g/c \sim 90$ ps. The corresponding laser energy is hence of the order of 90 J.

2.2. Energy output stability

Before moving onto the more complex three-dimensional equations, it is worthwhile to extract from the simple 1D model information about the sensitivity of the longitudinal high-gain FEL dynamics with respect to the initial conditions. In fact, 3D runs in SASE mode are noticeably expensive in terms of computational resources, whereas 3D runs in steady-state approximation (i.e. assuming an infinite beam length and neglecting propagation effects) are more manageable.

Figure 4 presents a comparison of the output energy as a function of wiggler length in the quatum regime $\bar{\rho} = 0.2$. The reference case is the red line depicting the energy per unit beam length E/L_b for the steady-state case. It is possible to see the first pulse of the train of hyperbolic secants, which are the fingerprint of the steady-state dynamics (see Figure 1). The normalized energy peaks after 6 L_g to the value of 1, consistently with the adopted quantum scaling. The energy goes then back to zero, since radiation cannot escape the system, and it is reabsorbed by the electron beam. The other curves all refer to the case of a electron
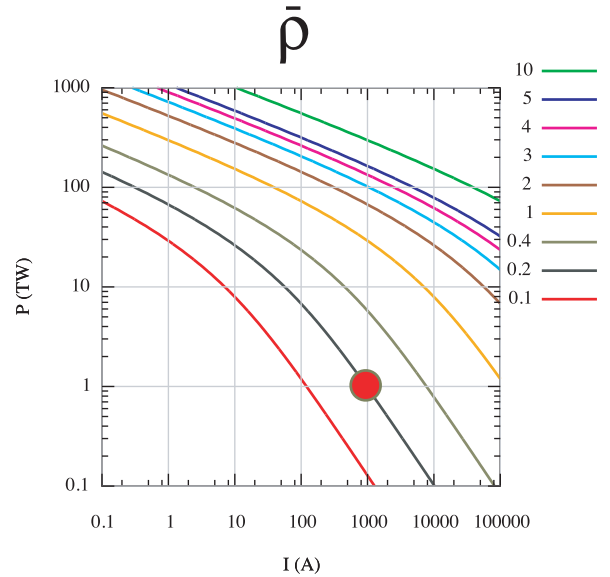

Fig. 2. Isocurves of the quantum FEL parameter $\bar{\rho}$ as a function of the beam current I and of the laser wiggler power P. The chosen working point for $\bar{\rho} = 0.2$ was set at $P = 1$ TW and $I = 884$ A. The other parameters can be found in the text.
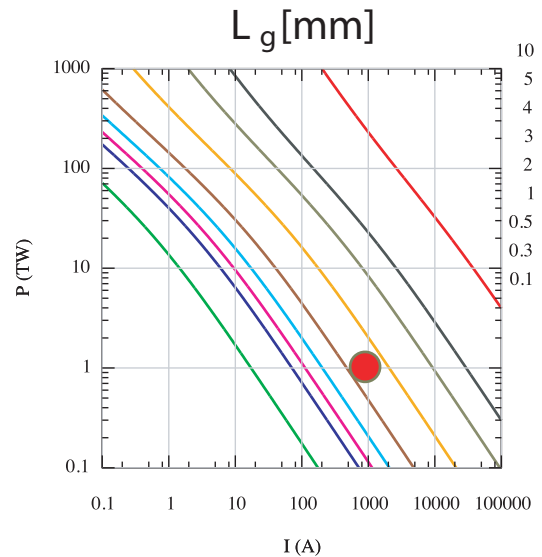

Fig. 3. Isocurves of the gain length L_g in the plane (I, P). The working point corresponds to $L_g = 1.3$ mm.

beam of finite length, namely $L_b = 20$ cooperation lengths. If a resonant coherent seed is injected (green curve), it is amplified by the FEL dynamics is a similar way to the steady-state resonant case. The peak value is lower than 1 because radiation is continuously escaping from the beam front, and therefore leaves the amplification medium. For

$z \geq 8$ the energy does not go to zero as in the infine-beam case, and a second peak start to appear. This is due to the super-radiant spike starting from the tail of the beam, and progressively converting beam momentum into radiation energy. This fact is clear in the blue curve representing the case of a non-resonant coherent seed. Here the seed is not amplified, and only the super-radiant spike instability is growing, leading to a peak at $\bar{z} \sim 10$. The last curve (black line with error bars) depicts the output energy averaged over 100 different SASE runs, where no seed was injected and the phase of the bunching was varied randomly along the beam. The normalized energy peaks in SASE mode after 9 gain lengths, and reaches about the 65% of the reference steady-state case. It is important to note that the energy fluctuations at saturation are of the order of 10%. In order to investigate the properties of the energy output as a function of the beam length, a series of simulations was performed varying the L_b parameter only, from 1 up to 1000 cooperation lengths. The energy curves were stacked up with increasing beam length, and presented in Figures 5 and 6 as color maps for the normalized energy E/L_b. When a resonant coherent seed was injected (Figure 5), the system follows the steady state dynamics for $L_b \geq 50$, peaking at 1 after 6 gain lengths. Finite beam effects, such as energy loss from the front and the super-radiant instability, become significant for beam lengths shorter than 20 cooperation lengths. The average output of SASE operation mode (Figure 6) indicates that the system can deliver up to 70% of the reference energy for $L_b \geq 50$ after 9 gain lengths. More noticeably the energy fluctuations become lower than 10% for $L_b \geq 20$. In summary, this set of simulations shows that for the case at study, i.e. for a beam with $L_b = 586$, the steady-state solution of the equations can be used to obtain a good estimation of both the output energy and the required wiggler length for saturation. As a rule of thumb, the SASE output will reach up to 70% of the steady-state output, but will need a longer wiggler. In our case, the radiated energy peaks before 10 gain lengths, so that the required interaction length $L_{int} = 10L_g$ is adequate for SASE operation.

3. 3D simulations

The one-dimensional QFEL model describing the quantized longitudinal dynamics between radiation and electrons was expanded including the transverse dynamics (7). This new set of equations allow the electron beam to focus and expand after passing through the waist, and the radiation to diffract away from the lasing volume. The transverse profile of the laser wiggler was also explicitly included, since the radius of the beam and that of the laser focal spot are comparable for the chosen working point.

Three new terms were added to the electron equation (1), which becomes

$$\frac{\partial w_s}{\partial \bar{z}} = - \left[\frac{s}{\bar{\rho}^{3/2}} + \bar{\delta} + \frac{\xi}{2\rho\sqrt{\bar{\rho}}}(1 - |g|^2) - \frac{b^2}{4a}\bar{p}_t^2 \right] \frac{\partial w_s}{\partial \theta}$$
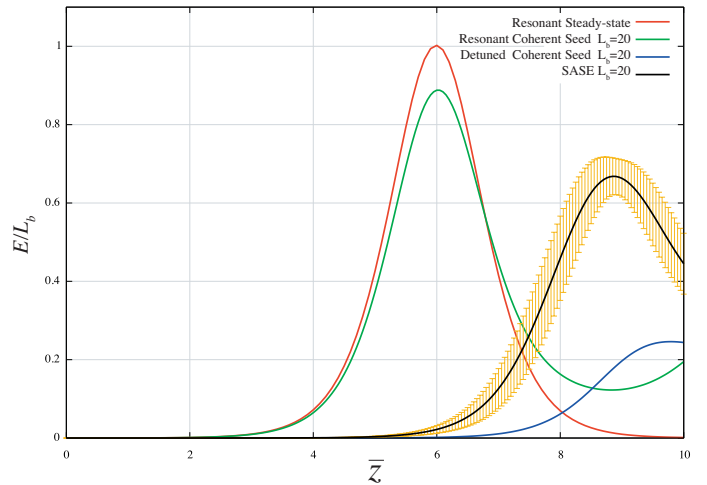

Fig. 4. Normalized radiation energy E/L_b as a function of wiggler length for the following cases: steady-state mode (red curve), resonant coherent seed (green), non-resonant coherent seed (blue), SASE mode averaged over 100 shots (black line with error bars). The last three cases are for a beam 20 cooperation lengths long.
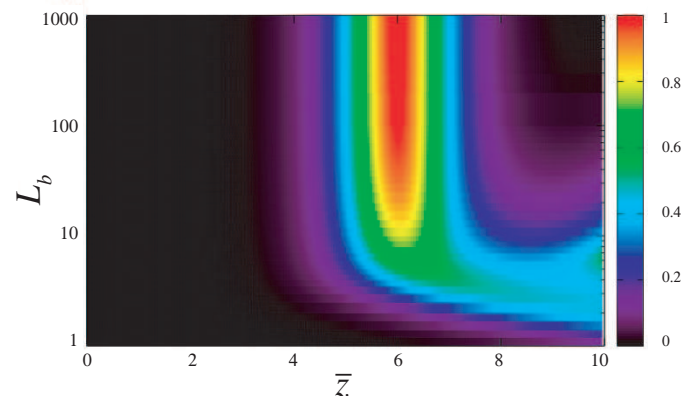

Fig. 5. Normalized radiation energy E/L_b as a function of wiggler length and of beam length for the case of a resonant coherent seed.
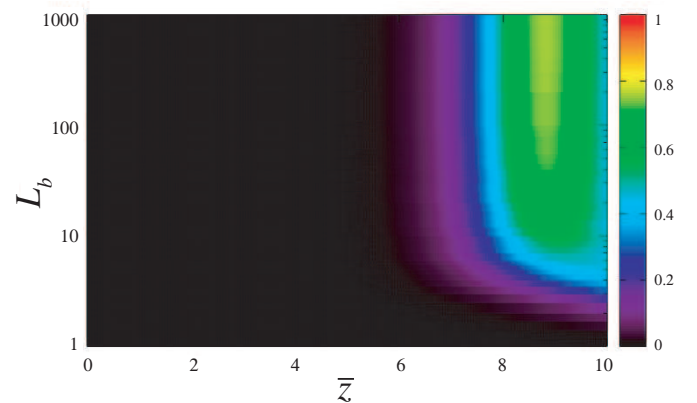

Fig. 6. Normalized radiation energy E/L_b as a function of wiggler length and of beam length averaged over 100 SASE runs.

$$+\left(g^*Ae^{i\theta} + gA^*e^{-i\theta}\right)\left(w_{s+\frac{1}{2}} - w_{s-\frac{1}{2}}\right)$$
$$-b\,\bar{\mathbf{p}}_t \cdot \nabla_{\bar{\mathbf{x}}_t} w_s \ , \tag{5}$$

where $\bar{\mathbf{x}}_t = \mathbf{x}_t/\sigma$ is normalized transverse vector and $\bar{\mathbf{p}}_t$ is the corresponding transverse momentum as defined in (7). Moreover $a = L_g/Z_r$ is the diffraction parameter, and $Z_r = 4\pi\sigma^2/\lambda$ is the Rayleigh range of the emitted radiation with a transverse radius equal to the electron beam radius. The emittance parameter is $b = L_g/\beta^*$, where $\beta^* = \sigma^2\gamma_r/\epsilon_n$ and ϵ_n is the normalized beam transverse emittance. The parameter $\xi = a_0^2/(1 + a_0^2)$ is related to the laser wiggler parameter a_0, and the laser transverse profile is described by $g(\bar{\mathbf{x}}_t, \bar{z})$. It can be seen that setting $b = 0$ and $g \equiv 1$, i.e. for a collimated beam and a uniform wiggler, equation (5) reduces to the one-dimensional beam equation.

The field equation was extended by adding a diffraction term proportional to the a parameter, and the source term due to the beam bunching was integrated over the transverse momentum and weighted according to the transverse wiggler profile g

$$\frac{\partial A}{\partial \bar{z}} + \frac{\partial A}{\partial z_1} - ia\nabla_{\bar{\mathbf{x}}_t}^2 A = g\sum_{m\in\mathbb{Z}}\int d^2\bar{\mathbf{p}}_t\int_{-\pi}^{+\pi}d\theta e^{-i\theta}w_{m+\frac{1}{2}}. \tag{6}$$

In the simulations the initial electron beam was described by a thermal state of energy $mc^2\gamma$, and the transverse phase space distribution w_0 was set proportional to $\exp\{-|\bar{\mathbf{x}}_t + b\bar{z}_0\bar{\mathbf{p}}_t|^2/2 - |\bar{\mathbf{p}}_t|^2/2\}$. Setting $a_0 = 0$ and therefore switching off the FEL interaction, it was checked that the $b\,\bar{\mathbf{p}}_t\cdot\nabla_{\bar{\mathbf{x}}_t}w_s$ term correctly describes the evolution of a gaussian beam with the waist position at $\bar{z} = \bar{z}_0$, and whose beam section scales as $\sigma(z) = \sigma\sqrt{1 + [(z - z_0)/\beta^*]^2}$ in free space.

In order to address the relative importance of the new transverse terms introduced in the model as well as the differences between 1D and 3D evolution, we investigated separately the effects of each term by switching off deliberately the others in the simulations. Let us rewrite the beam equation as

$$\frac{\partial w_s}{\partial \bar{z}} = -\left[\frac{s}{\bar{\rho}^{3/2}} + \bar{\delta} + \chi\left(1 - |g|^2\right) - \eta\,\bar{p}_t^2\right]\frac{\partial w_s}{\partial \theta}$$
$$+\left(g^*Ae^{i\theta} + gA^*e^{-i\theta}\right)\left(w_{s+\frac{1}{2}} - w_{s-\frac{1}{2}}\right)$$
$$-b\,\bar{\mathbf{p}}_t \cdot \nabla_{\bar{\mathbf{x}}_t} w_s \ , \tag{7}$$

where, for sake of clarity, we introduced $\chi = \frac{\xi}{2\rho\sqrt{\rho}}$ and $\eta = \frac{b^2}{4a}$. In the following we present the dependence of the emitted radiation energy on the laser wiggler profile g, on the resonance detuning induced by change of the wiggler parameter, and of the detuning caused by the beam emittance.

3.1. *Laser wiggler profile*

Firstly the case of a `TEM`$_{00}$ Gaussian laser wiggler was studied. Here the laser amplitude was set to
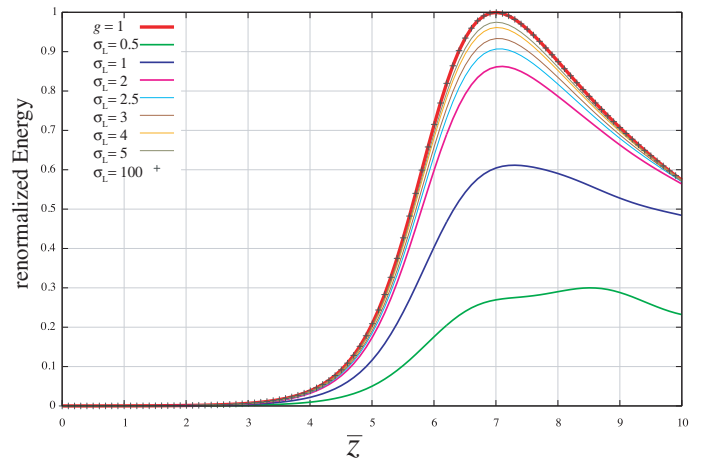

Fig. 7. Radiation energy as a function of wiggler position varying the laser wiggler focal spot $\sigma_L = R/\sigma$. The reference case (thick red line) corresponds to a uniform wiggler.
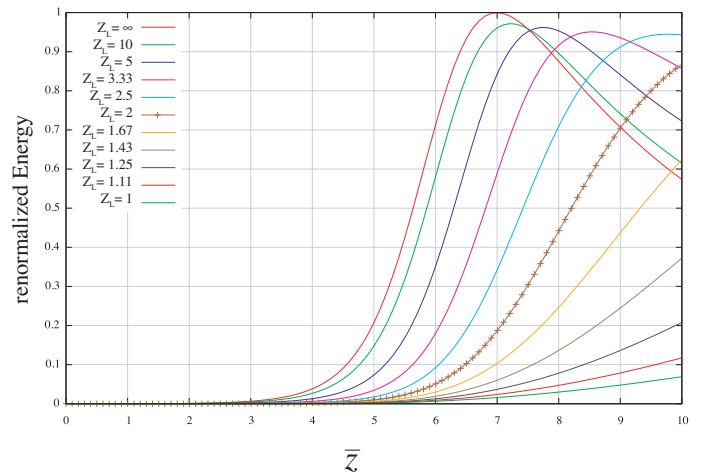

Fig. 8. Radiation energy as a function of wiggler position varying the laser wiggler Rayleigh range $\bar{Z}_L = Z_L/L_g$. Energy saturation occurs before the wiggler end for $\bar{Z}_L \geq 2$.

$$g(\bar{\mathbf{x}}_t, \bar{z}) = \frac{1}{[1 - i(\bar{z} - \bar{z}_0)/\bar{Z}_L]}\exp\left[\frac{-|\bar{\mathbf{x}}_t|^2}{4\sigma_L^2[1 - i(\bar{z} - \bar{z}_0)/\bar{Z}_L]}\right] \tag{8}$$

where $\sigma_L = R/\sigma$, $\bar{Z}_L = Z_L/L_g$, $Z_L = 4\pi R^2/\lambda_L$, R is the minimum rms laser radius, and the focal plane is located at the beam waist position $\bar{z}_0$. Figure 7 presents a series of 3D steady-state simulations highlighting the dependance of the emitted radiation on the ratio of the laser radius over the beam waist. Here we neglected emittance and diffraction effects (a and $b = 0$), and the laser was not diverging ($\bar{Z}_L = \infty$). We chose as reference case (red line) that of a uniform wiggler $g = 1$, corresponding to a focal spot of infinite radius $\sigma_L = \infty$. The renormalized energy peaks after 7 gain lengths, instead of 6 as in 1D steady-state case, due to the fact that the gain is lower in the beam halo and therefore saturation occurs there later on in the wiggler. It can be seen that, when the laser radius is 5 times the beam waist, $\sigma_L = 5$, the system can recover up to 98% of the energy output given by a uniform wiggler. For $\sigma_L = 2$ the output
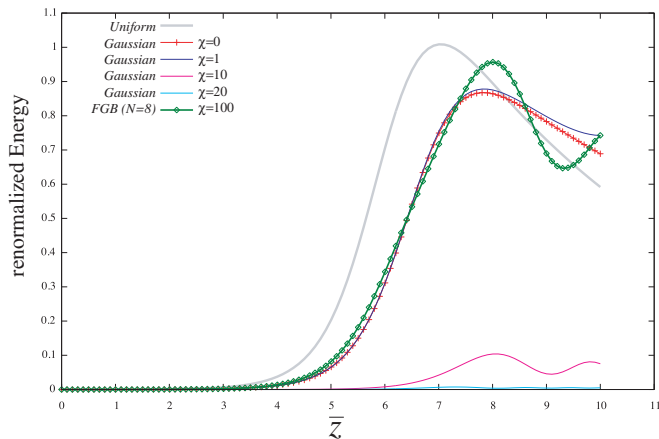
Fig. 9. Radiation energy as a function of wiggler position for different laser wiggler configurations. The reference case $g = 1$ is plotted in light gray. The effects of resonance detuning due to the χ term is presented for a Gaussian beam with $\chi = 0, 1, 10, 20$, and for a flat-top laser pulse (green line with diamonds) with $\chi = 100$.

reaches 86% of the uniform case, whereas for tighter focal spots the energy output drops considerably. By varying the divergence of the laser wiggler (see Figure 8), it can be seen that for a laser with Rayleigh range longer than 5 gain lengths, $\bar{Z}_L > 5$, the extracted energy is more than 95% of the reference. For this set of parameters, the case $\bar{Z}_L = 2$ can be considered as marginal, since the energy cannot reach saturation within the prescribed interaction length.

The χ factor can have a dramatic effect on the FEL dynamics, since near the chosen working point it can be found that $\chi \gtrsim 100$. This means that the term $\chi(1 - |g|^2)$ rapidly brings out of resonance the electrons where the laser amplitude drops from its maximum value, both radially and longitudinally. Figure 9 shows that for a Gaussian beam and for $\chi = 10$ the system goes already out of resonance. In order to overcome this problem, a laser with a tailored transverse profile could be used. We adopted the flattened Gaussian beam (FGB) proposed in (15). The amplitude $g(r, \bar{z})$ of an FGB is presented in Figure 9. By using a FGB of relatively lower order $N = 8$, it was possible to recover more than 95% of the reference energy even in the case of $\chi = 100$, as shown in Figure 9.

3.2. *Detuning caused by emittance and diffraction*

In the beam equation (7) the term proportional to $\eta = \frac{b^2}{4a}$ is responsible for FEL resonance detuning induced by the combined effects of beam emittance and of radiation field diffraction. A sensitivity study was carried out near the working point by varying the value of η, and observing the energy output of the system in steady-state operation. Figure 11 shows that η must be less than unity in order to preserve the resonance condition. Giving that at the working point the field diffraction parameter a is 1.6×10^{-4}, the emittance parameter b must be less than 0.025,
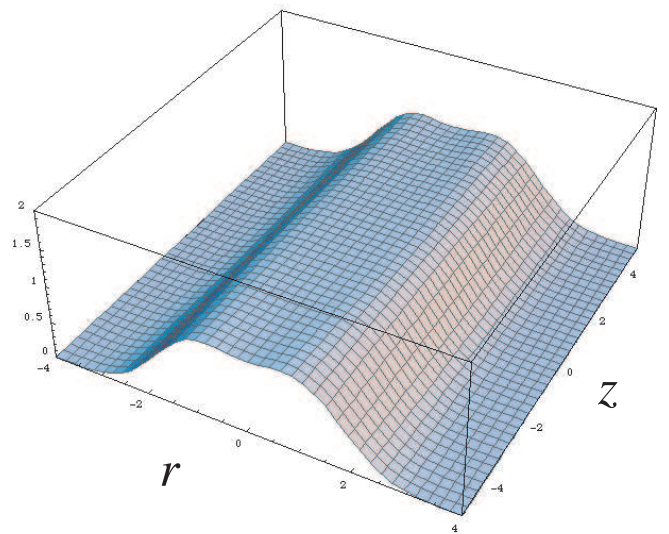

Fig. 10. Laser field amplitude $|g(r, z)|$ for a Flattened Gaussian Beam of order $N = 4$.
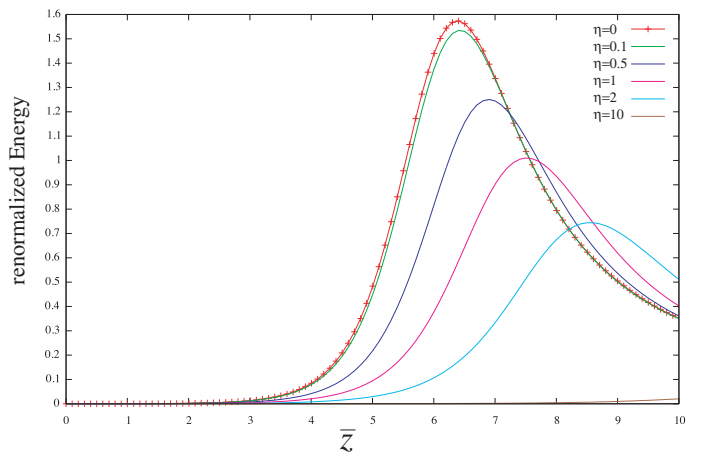

Fig. 11. Dependence of the radiation energy on the emittance and diffraction effects for different values of the factor $\eta = 0, 0.1, 0.5, 1, 2, 10$.

which correspondes in our case to an upper limit on the normalized emittance $\epsilon_n < 0.07$ mm-mrad.

4. Conclusions

In summary, we have presented a series of 3D simulations for a quantum FEL with a laser wiggler, including in the computation the effects of beam emittance and of radiation diffraction. The spatial profile of the laser field was explicitly taken into account, as well as the beam envelope evolution. Analysing the energy stability of a series of SASE runs, it was found that the steady-state solution of the QFEL dynamics can used as a reliable indication of the average energy output of a typical SASE shot, when the beam is many cooperation lengths long, $L_b > 50$, as in our reference case. Using a Gaussian pulse for the laser wiggler, it was found that up to 80-90% of the uniform wiggler energy output could be obtained if the Rayleigh range Z_L is

longer then $5L_g$ and the laser rms radius R is between 2 and 5 times the beam waist σ. The resonance detuning induced by the spatial variation of the wiggler parameter a_0 can have dramatic effects for tightly focussed Gaussian laser pulses. A possible cure would be to employ pulse tailoring techniques, which can produce flatter pulse profiles in the radial direction without introducing excessive phase fluctuations in the laser field. Finally it was found that beam emittance and field diffraction effects can have a significant impact on the system performance. For our working point, a stringent requirement was found on the normalized emittance of the beam, namely $\epsilon_n \leq 0.07$ mm-mrad.

References

[1] R. Bonifacio, N. Piovella, G.R.M. Robb, Nucl. Instrum. and Meth. in Phys. Res. A 543, 645 (2005).

[2] R. Bonifacio, N. Piovella, G.R.M. Robb, and A. Schiavi, Phys. Rev. ST Accel. Beams 9, 090701 (2006).

[3] Technical Design Report of the European X-ray Laser Project XFEL available at http://xfel.desy.de/tdr/tdr

[4] The LCLS Design Study Group: LCLS Design Study Report, SLAC-R521, Stanford (1998) and http://www-ssrl.slac.stanford.edu/lcls/CDR.

[5] T. Shintake, Status of the SCSS Test Accelerator and XFEL Project in Japan, EPAC'06, Edinburgh (2006) and http://www-xfel.spring8.or.jp.

[6] R. Bonifacio, N. Piovella, M.M. Cola, L. Volpe, A. Schiavi, and G.R.M. Robb, in these Proceedings.

[7] M.M. Cola, L. Volpe, N. Piovella, A. Schiavi, and R. Bonifacio, in these Proceedings.

[8] R. Bonifacio, Nucl. Instrum. and Meth. in Phys. Res. A 546, 634 (2005).

[9] R. Bonifacio, M. Ferrario, G.R.M. Robb, N. Piovella, A. Schiavi, L. Serafini, Proceedings of the 27th International Free Electron Laser Conference, 71 (2005).

[10] R. Bonifacio, N. Piovella, M.M. Cola, and L. Volpe, Nucl. Instrum. and Meth. in Phys. Res. A577 (2007) 745.

[11] W.H. Press and S.A. Teukolsky and others, *Numerical Recipes in C - The Art of Scientific Computing - Second Edition* , Cambridge University Press, USA (1994).

[12] T. Yabe and T. Aoki, *Comp. Phys. Commun.* **66**, 219 (1991).

[13] R. Bonifacio, M.M. Cola, R. Gaiba, L. Volpe, N. Piovella, and A. Schiavi, Opt. Commun. 274, 347 (2007).

[14] J.P. Bizarro, Phys. Rev. A 49, 3255 (1984).

[15] F. Gori, Opt. Commun. 107, 335 (1994); V. Bagini et al., J. Opt. Soc. Am. A 13, 1385 (1996).